

Gravitational D -Form Factor: The σ -Meson as a Dilaton confronted with Lattice Data

Roy Stegeman and Roman Zwicky

Higgs Centre for Theoretical Physics, The University of Edinburgh, Peter Guthrie Tait Road,
Edinburgh EH9 3FD, Scotland, UK

Email: r.stegeman@ed.ac.uk, roman.zwicky@ed.ac.uk

We investigate the nucleon and pion gravitational D -form factors, by fitting a $\sigma/f_0(500)$ -meson pole, together with a background term, to lattice data at $m_\pi \approx 170$ MeV. We find that the fitted residues are compatible with predictions from dilaton effective theory. In this framework, the σ -meson takes on the role of the dilaton, the Goldstone boson of spontaneously broken scale symmetry. These results support the idea that QCD may be governed by an infrared fixed point and offer a physical interpretation of the D -form factor (or D -term) in the soft limit.

Contents

1. Introduction	2
2. Gravitational Form Factors	3
2.1. Definition of nucleon and pion form factors	3
2.2. Leading order dilaton effective theory and $D(q^2)$	3
3. The σ-pole in the Euclidean	5
3.1. The effect of a resonance in the deep Euclidean	5
3.2. Fit ansatz	6
4. Numerics and Fits to Lattice Data at $m_\pi \approx 170$ MeV	7
4.1. The nucleon gravitational form factor	8
4.2. The pion gravitational form factor	10
4.3. A quick note on the D -form factor in the infrared - the D -term	12
5. Conclusions and Discussion	13
A. The Gell-Mann Lévy linear σ-model – a study case	14
A.1. The linear σ -model Lagrangian in the broken phase	15
A.2. Relevant NLO corrections	16
A.2.1. Self-energy corrections $\Sigma(s)$	16
A.2.2. Vertex corrections $v(s)$	17
A.3. Second-sheet analytic continuation of the form factor	18
A.4. Concluding the form-factor study in the linear σ -model	20
B. A Multipole Expansion in Momentum Space	21

1. Introduction

Gravitational form factors probe the energy-momentum tensor for physical states, such as nucleons, through matrix elements of the form $\langle N(p')|T_{\mu\nu}|N(p)\rangle$. The momentum transfer $q = p' - p$ reveals the energy-momentum distribution of the nucleon just like electromagnetic form factors test the charge distribution. Defined a long time ago [1, 2], gravitational form factors have seen a growing interest (reviewed in [3–6]). In part related to their experimental accessibility, through the first moment of generalised parton distributions [7], in deeply virtual Compton scattering [8, 9], near-threshold J/ψ photoproduction [10], and $\gamma^*\gamma \rightarrow \pi\pi$ [11–13], among others. This has triggered lattice QCD investigations [14–19] which provide the basis of this paper. In addition to experiment and lattice results, there are perturbative approaches in chiral theories at low q^2 [20, 21] and light-cone sum rules at high q^2 [22–26], dispersive analyses [27–30], Skyrme-based models [31–33], light-front quark models [34, 35], and holographic models [36–39].

Conserved-current form factors often obey physical constraints at zero momentum transfer. An example is the charged-pion electromagnetic form factor $F_+(0) = 1$, expressing charge conservation. The infrared interpretation of the gravitational D -form factor, associated with the internal pressure distribution [40], has remained elusive and puzzled the community for a long time [3, 6]. Our work offers an explanation in terms of the dilaton.

The idea that strong interactions are governed by an infrared fixed point [41–43] has recently been reexamined in QCD, both in low-energy processes [44, 45] and more formally [46–48], by matching scaling dimensions of the underlying theory to those of the effective theory. Consistency regarding the quark-mass anomalous dimension with lattice simulations [49–55] (or fits thereto [56, 57]), phenomenological models, lower dimensional models [58] and $\mathcal{N} = 1$ supersymmetric gauge theories [47, 59, 60] are established. The underlying idea of this scenario is that spontaneous scale symmetry breaking generates hadron masses, with the resulting Goldstone bosons, the dilaton, realising the corresponding Ward identities.¹

The gravitational form factors, for a scalar φ , provides the ideal setting to illustrate these ideas

$$\Theta_{\mu\nu}(q) \equiv \langle \varphi(p')|T_{\mu\nu}(0)|\varphi(p)\rangle = 2\mathcal{P}_\mu\mathcal{P}_\nu A(q^2) + \frac{1}{2}(q_\mu q_\nu - q^2\eta_{\mu\nu})D(q^2), \quad (1.1)$$

with momenta $2\mathcal{P} \equiv p + p'$ and q as defined above. Energy conservation implies the model-independent constraint $A(0) = 1$ and if one assumes that $D(q^2)$ is regular for $q \rightarrow 0$, one recovers the standard textbook formula $\Theta(0) \equiv \Theta^\rho_\rho(0) = 2m_\varphi^2$. However, in the presence of a massless dilaton arising from spontaneous scale symmetry breaking, the dilaton pole

$$D(q^2) = \frac{4}{3}\frac{m_\varphi^2}{q^2} + \mathcal{O}(1), \quad (1.2)$$

modifies the textbook formula to satisfy the infrared conformal Ward identity “ $T^\rho_\rho = 0$ ”, analogous to the Goldberger-Treiman mechanism, where the pion restores the chiral Ward identity [67].² Consequently, one finds

$$\Theta(0) = \langle \varphi(p)|T^\rho_\rho(0)|\varphi(p)\rangle = \begin{cases} 2m_\varphi^2 & \text{textbook formula} \\ 0 & \text{dilaton pole} \end{cases}. \quad (1.3)$$

¹Gauge theories dilatons are of interest elsewhere, e.g. the Higgs as a dilaton [61–63] or nuclear physics [64–66].

²In the axial singlet channel, the η' plays a similar role in QCD processes, see for instance [68]. For the dilaton it was proposed in ref. [69], and verified using the LSZ formalism [70] and the effective theory [71].

In this work, we test infrared conformality in a direct and physical way, independent of β -functions. Our strategy is to fit lattice data for the nucleon and pion gravitational D -form factor [16, 17] to the predictions of leading-order (LO) dilaton effective theory [71], which incorporates the dilaton Goldberger-Treiman mechanism described above.

The paper is organised as follows. In section 2 the gravitational form factors are defined for the nucleon and pion, and the LO dilaton predictions are given. Section 3 motivates a fit ansatz suitable in the Euclidean regime. In section 4 we present our fits, test the dilaton hypothesis and comment on the D -term. Conclusions and discussions follow in section 5. Appendix A explores the linear σ -model to clarify the relation between complex-valued and effective Euclidean poles, while appendix B sketches a multipole expansion in momentum space to motivate the fit ansatz.

2. Gravitational Form Factors

2.1. Definition of nucleon and pion form factors

The gravitational form factors of the nucleon N and the pion π are defined, in the now-standard conventions, as

$$\begin{aligned} \langle N(p', s') | T_{\mu\nu} | N(p, s) \rangle &= \frac{1}{2m_N} \bar{u}(p', s') \left(a_{\mu\nu} A^N(q^2) + j_{\mu\nu} J^N(q^2) + d_{\mu\nu} D^N(q^2) \right) u(p, s) , \\ \langle \pi(p') | T_{\mu\nu} | \pi(p) \rangle &= \left(a_{\mu\nu} A^\pi(q^2) + d_{\mu\nu} D^\pi(q^2) \right) , \end{aligned} \quad (2.1)$$

where $u(p, s)$ denotes the Dirac spinor, with $(\sigma_{\mu\nu} = \frac{i}{2}[\gamma_\mu, \gamma_\nu])$ and $\sigma_{q\nu} = \sigma_{\mu\nu} q^\mu$

$$a_{\mu\nu} = 2\mathcal{P}_\mu \mathcal{P}_\nu , \quad d_{\mu\nu} = \frac{1}{2}(q_\mu q_\nu - q^2 \eta_{\mu\nu}) , \quad j_{\mu\nu} = 2i \mathcal{P}_\mu \sigma_{q\nu} + \mu \leftrightarrow \nu , \quad (2.2)$$

Lorentz structures ensuring translational invariance $q^\mu \Theta_{\mu\nu}(q) = 0$. The normalisation $A(0) = 1$ holds model-independently since $T_{\mu\nu}$ is the associated Noether current with conserved momenta $P_\mu = \int d^3x T_{\mu 0}$. Furthermore, for the nucleon one has $J^N(0) = \frac{1}{2}$, which reflects the absence of an anomalous gravitational magnetic moment, a consequence of the universality of gravity.³

2.2. Leading order dilaton effective theory and $D(q^2)$

The form factors have been evaluated in the LO dilaton effective theory in an arbitrary space-time dimension d , including chiral corrections, in ref. [71]. Here, we consider it instructive to highlight the main effect, the dilaton pole in the D -form factor, using the nucleon as an example. Denoting the dilaton by σ and the coset field by $\hat{\chi} = e^{-\sigma/F_\sigma}$, the relevant Lagrangian reads

$$\mathcal{L}_{\text{eff}} = \frac{1}{2} F_\sigma^2 ((\partial \hat{\chi})^2 - \frac{1}{6} R \hat{\chi}^2) + \hat{\chi}^{3-2\omega_N} \bar{N} (i \not{\Delta} - \hat{\chi} m_N) N , \quad (2.3)$$

where F_σ , R , ω_N and Δ_μ stand for the dilaton decay constant, the Ricci scalar, the nucleon Weyl weight (conformal charge) and the Weyl-covariant derivative, respectively. For the latter we refer the reader to original refs. [41, 72, 73], and [71] for an emphasis on generic Weyl-weight.

³The form factors $A^{\pi, N}$ and J^N are the analogues of the electromagnetic pion, Dirac and Pauli form factors.

We first focus on the improvement term proportional to the Ricci scalar. While irrelevant for scattering in flat space, it contributes to the energy-momentum tensor

$$T_{\mu\nu} \supset T_{\mu\nu}^R = \frac{F_\sigma}{6} (\eta_{\mu\nu} \partial^2 - \partial_\mu \partial_\nu) \hat{\chi}^2, \quad (2.4)$$

since it is an effective coupling to gravity. It is crucial as it realises the Goldstone matrix element in the effective theory

$$\langle 0 | T_{\mu\nu}^R | \sigma \rangle = \frac{F_\sigma}{3} (m_\sigma^2 \eta_{\mu\nu} - q_\mu q_\nu), \quad (2.5)$$

which defines F_σ as the order parameter of spontaneous scale-symmetry breaking. This term contributes to the D -form factor, via a single dilaton exchange with the nucleon pair, parametrised by the on-shell interaction

$$\delta \mathcal{L}_{\text{eff}} = g_{\sigma NN} \sigma \bar{N} N, \quad g_{\sigma NN} = \frac{m_N}{F_\sigma}. \quad (2.6)$$

This result, derived from (2.3), is independent of the Weyl-weight and realises the Goldberger-Treiman mechanism (1.2) for the dilaton, as one readily obtains

$$D^N(q^2) = \frac{r_\sigma^N}{q^2}, \quad r_\sigma^N = \frac{2}{3} \bar{u}(p) u(p) F_\sigma g_{\sigma NN} = \frac{4}{3} m_N^2, \quad (2.7)$$

using $\bar{u}(p) u(p) = 2m_N$.

The full LO computation, including linear quark mass effects, reads [71]

$$D^N(q^2) = \frac{4}{3} \frac{\bar{m}_N^2}{q^2 - m_\sigma^2}, \quad D^\pi(q^2) = \frac{2}{3} \frac{q^2}{q^2 - m_\sigma^2} - 1, \quad (2.8)$$

where \bar{m}_N denotes the nucleon mass in the chiral limit. The physical nucleon mass can then be written as

$$m_N = \bar{m}_N + \Delta m_N, \quad (2.9)$$

with Δm_N the non-vanishing part due to $m_{u,d,s} \neq 0$. In the nucleon case the linear quark corrections vanish since the residue is of the form $m_N(\bar{m}_N - \Delta m_N) = \bar{m}_N^2 - (\Delta m_N)^2$. Hence, further contributions are of $\mathcal{O}(m_q^{3/2})$ as in ordinary nucleon chiral perturbation theory [74]. The corrections in the pion case are $\mathcal{O}(m_\pi^4 \ln m_\pi)$ as usual. In the pion case it is worthwhile to point out that there is a soft-pion theorem constraining the LO trace to be [71, 75]

$$\Theta^\pi(q^2) = \begin{cases} 2m_\pi^2 + q^2 & m_{\pi,\sigma} \neq 0 \\ 0 & m_{\pi,\sigma} = 0 \end{cases}, \quad (2.10)$$

and contracting (1.1) this needs to match the expression

$$\Theta^\pi(q^2) = 2m_\pi^2 A^\pi(q^2) - \frac{q^2}{2} (A^\pi(q^2) + 3D^\pi(q^2)). \quad (2.11)$$

Together with the model-independent normalisation $A^\pi(0) = 1$, this implies the constraints⁴

$$\left\{ \begin{array}{ll} D^\pi(0) = -1, & m_{\pi,\sigma} \neq 0 \quad [75] \\ D^\pi(0) = -\frac{1}{3}, \quad r_\sigma^\pi = \mathcal{O}(q^2), & m_{\pi,\sigma} = 0 \quad [71] \end{array} \right. , \quad (2.12)$$

subject to higher order chiral corrections. We emphasise that, for nonzero pion mass, the constraint holds independently of any fixed-point interpretation and is therefore directly relevant for the present work. In fact, Donoghue and Leutwyler [75] employed the soft theorem together with the σ -meson dominance assumption to deduce this form. Consequently, the constraint $D^\pi(0) = -1$ provides a valuable handle for fixing the fit ansatz of the pion. In contrast, for the nucleon no analogous constraint exists, since constant or q^2 -dependent shifts may arise from higher resonances or multi-particle contributions to the spectrum.

3. The σ -pole in the Euclidean

Our primary fit ansatz consists of a σ -pole contribution together with a simple background term

$$D(q^2) = \sigma\text{-pole} + \text{background} . \quad (3.1)$$

Describing the σ -pole is a non-trivial task since the σ -meson is perhaps the most complicated and mysterious resonance of QCD [76] and its pole is deep in the complex plane on the second sheet [77]

$$\sqrt{s_\sigma} = m_\sigma - \frac{i}{2}\Gamma_\sigma = (441_{-8}^{+16} - i272_{-12.5}^{+9}) \text{ MeV} . \quad (3.2)$$

Our main point is that the details of the σ -meson in the Minkowski domain are irrelevant in the deep Euclidean region, where a simple effective pole parametrisation proves sufficient. In section 3.2, we will revisit the issue and explain why alternative resonance parameterisations are not well suited.

3.1. The effect of a resonance in the deep Euclidean

Let us consider a generic form factor

$$G(q^2) = \langle H(p') | \mathcal{O} | H(p) \rangle , \quad (3.3)$$

where \mathcal{O} denotes the operator, transitioning from $H(p)$ to $H(p')$, and coupling to a stable particle φ in the $q^2 = (p - p')^2$ channel. If we assume that $G(q^2)$ is real for $q^2 < m_\varphi^2$ (real analyticity), then it admits a dispersion representation of the form

$$G(q^2) = \int_0^\infty \frac{ds \rho_G(s)}{s - q^2 - i0} = \frac{r_{0,\varphi}}{q^2 - m_\varphi^2} + \delta G(q^2) , \quad (3.4)$$

where $\rho_G(s) = \frac{1}{\pi} \text{Im} G(s)$ and $\delta G(s)$ encodes the remaining spectral contributions. In this case, the effect of the pole across the complex plane is simple and fully controlled by the residue $r_{0,\varphi}$. Now suppose we turn on a parameter that renders the particle φ unstable. The pole then

⁴ Alternatively, one may write $D^\pi(q^2)|_{\text{LO}} = \frac{2}{3} \frac{m_\sigma^2}{q^2 - m_\sigma^2} - \frac{1}{3}$, more natural from the dispersive viewpoint.

moves to the second sheet, $\sqrt{s_\varphi} = m_\varphi - \frac{i}{2}\Gamma_\varphi$, and one may define a complex-valued residue r_φ through

$$G^{(\text{II})}(q^2)|_{q^2 \approx s_\varphi} = \frac{r_\varphi}{q^2 - s_\varphi} + \mathcal{O}(1), \quad (3.5)$$

where the superscript indicates the second-sheet continuation. While this definition is interesting in its own right, it is not the relevant quantity for analyzing the pole contribution in the deep Euclidean region, since there the form factor remains real.

Intuitively, we expect

$$G(q^2)|_{q^2 \ll m_\varphi^2} \approx \frac{r_{\text{E},\varphi}}{q^2 - m_{\text{E},\varphi}^2} + \delta\tilde{G}(q^2), \quad (3.6)$$

where $r_{\text{E},\varphi}$ and $m_{\text{E},\varphi}$ denote effective Euclidean residue and mass, respectively. In particular, we anticipate

$$(i) \quad \arg(\sqrt{s_\sigma}) \leftrightarrow \arg(r_\varphi), \quad (ii) \quad r_{\text{E},\varphi} \neq |r_\varphi|, \quad (3.7)$$

that the phase in the pole correlates with the residue phase, and that the Euclidean residue can differ significantly from the modulus of the complex residue. More generally, one would expect $m_{\text{E},\varphi} \approx |s_\varphi|$ and that $|r_{\text{E},\varphi}/r_\varphi| < 1$. Both (i) and (ii) hold true in the linear σ -model, presented in appendix A, while the more qualitative features remain valid across a wide range of parameters. In addition, a more formal treatment of this idea, in the spirit of a multipole expansion in momentum space, is given in appendix B.

3.2. Fit ansatz

Since the lattice data are available in the Euclidean range $q^2 \in [-2, 0] \text{ GeV}^2$, we adopt the following parametrisation for the D -form factor, motivated by the discussion in the previous section

$$D(q^2) = \frac{r_{\text{E},\sigma}}{q^2 - m_{\text{E},\sigma}^2} + b(q^2). \quad (3.8)$$

In fact, it has been noted in the literature that σ -effects in the Euclidean domain are well approximated by a σ -pole with pole-mass in the range 500-600 MeV [78] (see also [27, 29]), further supported by the empirical success of one-boson-exchange models (e.g. [79, 80]). The fact that the up and down quark masses are expected to enlarge the real part of the complex pole might well be compensated by the reduction of the imaginary because of reduced phase space. We therefore ignore this effect and adopt $m_{\text{E},\sigma} = 550(50) \text{ MeV}$ as our central value. The parameter $r_{\text{E},\sigma}$ serves as our primary fit variable, to be tested against the prediction of dilaton effective theory.

The background contribution must of course be nonzero, as it accounts for higher states in the spectrum. In a spontaneously broken conformal theory, the dilaton (identified here with the σ -meson) is the only state that couples in the scalar channel, as follows from the textbook derivation of Goldstone's theorem [81]. By contrast, the situation is less clear in a theory flowing to an infrared fixed point with spontaneous breaking of scale invariance. In such a scenario, suppression of other states near the fixed point appears plausible, since in the effective theory they would be loop-suppressed, unlike for the dilaton.

Since the above reasoning is not entirely rigorous it is best to take an agnostic attitude and explicitly parametrise for a background. For this purpose we use a combination of the following terms

$$b(q^2) = b + b'q^2 + \frac{r_{\text{eff}}}{q^2 - m_{\text{eff}}^2}, \quad (3.9)$$

paying attention to avoiding over-parametrisation in view of the available data. Before presenting the fits, we digress to comment in more technical language why certain alternative parametrisations are not employed.

- (i) Are there viable alternatives to the Euclidean pole parametrisation? A first difficulty arises from the fact that, although the pole position itself is uniquely defined, the behaviour in its vicinity is not as it depends sensitively on the production mechanism or process under consideration. This issue is particularly relevant for the σ -meson, which is both broad (3.2) and located close to the left-hand cuts of $\pi\pi$ -scattering. These features explain why the σ phase shift does not pass rapidly through 180° ; see, for example, Fig. 2 in [76] or the discussion in [82]. Through Watson’s theorem, this behaviour directly carries over to the form-factor case, since the same phase enters both $\pi\pi$ -scattering and the form factor (via the Omnès representation [83]), see for instance [84, 85]. This property alone rules out many commonly used parametrisations, including all Breit–Wigner forms and Flatté-type (or “sill”) models [86]. While the sill model performs reasonably well for the moderately broad $a_1(1260)$ meson, it fails for the much broader $\kappa/K_0^*(700)$, which in fact shares important characteristics with the σ [86]. Other approaches, such as the K-matrix employed by the HadSpec collaboration at $m_\pi \approx 239$ MeV [87], or the single-resonance S -matrix solution of [82], are not suitable either, since they are designed for the S -matrix rather than for form factors. In scattering amplitudes, left-hand cuts are naturally included in these frameworks, which are absent in the form-factor case. A dispersive analysis using the Omnès representation [28, 30], is closer to extracting the complex-valued residue which is not what we are aiming at.
- (ii) It has been argued that in the deep Euclidean limit $q^2 \rightarrow -\infty$, the form factors scale as $D^\pi \propto 1/q^2$ and $D^N \propto 1/q^6$, based on light-cone sum rule computations [23, 24]; see also [88] for an instanton-based approach to the pion case. In the absence of further input, such asymptotic constraints can provide useful guidance for parametrisations [27, 29]. However, we choose not to impose them here for several reasons. First, it is not evident that $q^2 = -2$ GeV² should already be regarded as the deep Euclidean regime, and most of our relevant fit points are even less Euclidean. Second, the light-cone sum rule estimates rely heavily on the endpoint region of the corresponding distribution amplitudes, which are generally unknown and often assumed to take the asymptotic form. This assumption has been challenged by high- q^2 measurements of $\eta(\pi)\gamma\gamma^*$ transitions; see, for example, [89] and references therein.

4. Numerics and Fits to Lattice Data at $m_\pi \approx 170$ MeV

In this section, we fit our ansatz (3.8) to lattice data at $m_\pi \approx 170$ MeV [16, 17], close to the physical pion mass of $m_\pi \approx 140$ MeV. Our goal is to test whether the σ -meson ansatz naturally reproduces the σ -residue predicted by the dilaton interpretation Eq. (2.8). Attempting the converse, deriving the dilaton picture directly from the data, proves too challenging for the pion and only marginally feasible for the nucleon.

4.1. The nucleon gravitational form factor

The concrete fit ansatz for the nucleon gravitational form factor is

$$D^N(q^2) = \frac{r_{\text{E},\sigma}^N}{q^2 - m_{\text{E},\sigma}^2} + b + b' q^2 + \frac{r_{\text{eff}}}{q^2 - m_{\text{eff}}^2}, \quad (4.1)$$

where we fix $m_{\text{eff}} = 1 \text{ GeV}$ to account for the effect of the $f_0(980)$ resonance and additional higher states in the spectrum. In our main fit we set $r_{\text{eff}} = 0$, while alternative combinations are used to test the robustness of the procedure. Since our primary goal is to compare the fit result with the dilaton prediction $r_{\sigma}^N = \frac{4}{3} \bar{m}_N^2$ (2.8), we need to estimate its central value and associated uncertainty. Here, \bar{m}_N denotes the nucleon mass in the limit of vanishing $m_{u,d,s}$, for which we adopt the value $\bar{m}_N = 826 \text{ MeV}$ from the recent pedagogical introduction [90].⁵ This corresponds to a 13% reduction from the physical nucleon mass, $m_N \approx 938 \text{ MeV}$, with a significant part arising from the nucleon's strangeness content. As discussed earlier, the leading parametric corrections are radiative, of order $\mathcal{O}(m_q^{3/2})$, and are known to induce a negative shift of about 15 MeV in the $SU(2)$ chiral perturbation theory [92]. Since the strange-quark contribution is comparable to that of the other light quarks, we assume a similar size for the radiative corrections and therefore double the uncertainty. In addition, one expects q^2 -dependent corrections. For small q^2 these can be estimated within the effective theory, and their asymptotic behaviour suggests that they are not large (see the discussion in section 3.2). Such effects are absorbed into the background and are therefore, in principle, accounted for by the model uncertainty. To be conservative, we add an additional 10% uncertainty, which combined in quadrature with the other effects yields the following estimate

$$r_{\sigma}^N|_{\text{dilaton}} = 0.91(12) \text{ GeV}^2. \quad (4.2)$$

For the fit, we minimise the χ^2

$$\chi^2 = \sum_{i,j=1}^{N_{\text{data}}} (D_{\text{data}}^N - D_{\text{model}}^N)_i (\text{Cov}^{-1})_{ij} (D_{\text{data}}^N - D_{\text{model}}^N)_j, \quad \hat{\chi}^2 \equiv \frac{\chi^2}{N_{\text{dof}}}, \quad (4.3)$$

using all 33 available data points [16]. The effective number of degrees of freedom is $N_{\text{dof}} = 30$ since there are three fit parameters. A fit using the main parametrisation is displayed in the left figure of Fig. 1, where it is compared to the data of ref. [16]. Table 1 shows the corresponding fit parameters for a range of effective σ -masses, and the uncertainties correspond to the standard deviations as encoded in the covariance matrix. The covariance matrix of the fitted parameters is estimated from the inverse χ^2 -Hessian, evaluated at the χ^2 -minimum.

We identify two primary sources of uncertainty: the data itself and the choice of $m_{\text{E},\sigma}$. The data uncertainty is propagated to the fit parameters through the fit procedure, while the dependence on $m_{\text{E},\sigma}$ can be assessed by varying its value within $m_{\text{E},\sigma} = 550(50) \text{ MeV}$. The background parameters b and b' are treated as nuisance parameters in the fit, and their variation is accounted for in the quoted uncertainty on $r_{\text{E},\sigma}^N$.

The final result is

$$r_{\text{E},\sigma}^N = 1.13(26)(20) \text{ GeV}^2, \quad (4.4)$$

which is consistent with the dilaton prediction given in (4.2).

⁵Combining the uncertainties from the light and strange quark masses in quadrature gives a total uncertainty of roughly 10 MeV, which is small. One should, however, remain mindful of the longstanding tension between phenomenology and lattice results regarding light quark contributions [91].

$m_{E,\sigma}$ [MeV]	$r_{E,\sigma}^N$ [GeV ²]	b	b'	χ^2/N_{dof}
450	0.83(19)	0.44(30)	0.10(13)	0.55
500	0.97(22)	0.56(32)	0.13(14)	0.55
550	1.13(26)	0.69(35)	0.17(14)	0.55
600	1.32(30)	0.84(38)	0.21(15)	0.56
650	1.54(35)	0.99(42)	0.25(16)	0.56

Table 1: Model parameters for the nucleon D -form factor resulting from fits using our main background parametrisation, and for various values of the pole mass $m_{E,\sigma}$, to the 33 lattice data points at $m_\pi \approx 170$ MeV [16]. The uncertainties correspond to the standard deviations encoded in the covariance matrix. The correlations between parameters are $(\rho_{rb}, \rho_{rb'}, \rho_{bb'}) = (0.97, 0.91, 0.98)$ for $m_{E,\sigma} = 550$ MeV. LO dilaton effective theory predicts $r_\sigma^N = 0.91(12)$ GeV² (4.2).

Let us turn to testing the robustness of the fit. Allowing all three background parameters to vary simultaneously leads to large marginalised uncertainties which would make a comparison to the dilaton prediction largely inconclusive. On the other hand, omitting the background entirely is theoretically disfavoured, as discussed above. Insisting on no background, the fit yields $r_{E,\sigma} = 0.476(34)$, with a χ^2 -value that is nearly double that of the main parametrisation, which indeed rules out this ansatz on its own. More reasonable combinations, fitted with a fixed $m_{E,\sigma} = 550$ MeV, are

- a) $(r_{E,\sigma}, b)^N$: with $r_{E,\sigma}^N = 0.86(11)$, $b = 0.291(77)$ and $\hat{\chi}^2 = 0.58$
- b) $(r_{E,\sigma}, b, r_{\text{eff}})^N$: with $r_{E,\sigma}^N = 1.55(58)$, $b = -0.04(28)$, $r_{\text{eff}} = -1.8(1.5)$ and $\hat{\chi}^2 = 0.55$
- c) $(r_{E,\sigma}, r_{\text{eff}})^N$: with $r_{E,\sigma}^N = 1.47(25)$, $r_{\text{eff}} = -1.57(39)$ and $\hat{\chi}^2 = 0.53$
- d) $(r_{E,\sigma}, b', r_{\text{eff}})^N$: with $r_{E,\sigma}^N = 1.53(45)$, $b' = 0.010(67)$, $r_{\text{eff}} = -1.68(84)$ and $\hat{\chi}^2 = 0.55$

Firstly, we note that all of these fits are compatible with the main result (4.4). Secondly, they also remain consistent with the theoretical prediction (4.2), particularly once the spread in the effective mass is taken into account. Fits c) and d) provide a more direct test of the σ -meson dominance hypothesis, as the r_{eff} -residue could potentially account for the curvature in the data. We observe that, while r_{eff} is non-negligible, $r_{E,\sigma}^N$ continues to agree with the theoretical expectation. In conclusion, there is good agreement within uncertainties with the dilaton interpretation, and this last observation suggests that the reverse scenario, establishing σ -dominance, is not out of sight.

Now, the complex-valued residue has been determined using Roy-Steiner equations [93]. Their result and our fit to the Euclidean residue differ, also in their absolute values

$$r_\sigma^N |_{[93]} = (0.90(28) - 2.78(20)i) \left[\frac{4}{3} m_N^2 \right], \quad r_{E,\sigma}^N |_{(4.4)} \approx 1.04 \left[\frac{4}{3} m_N^2 \right]. \quad (4.5)$$

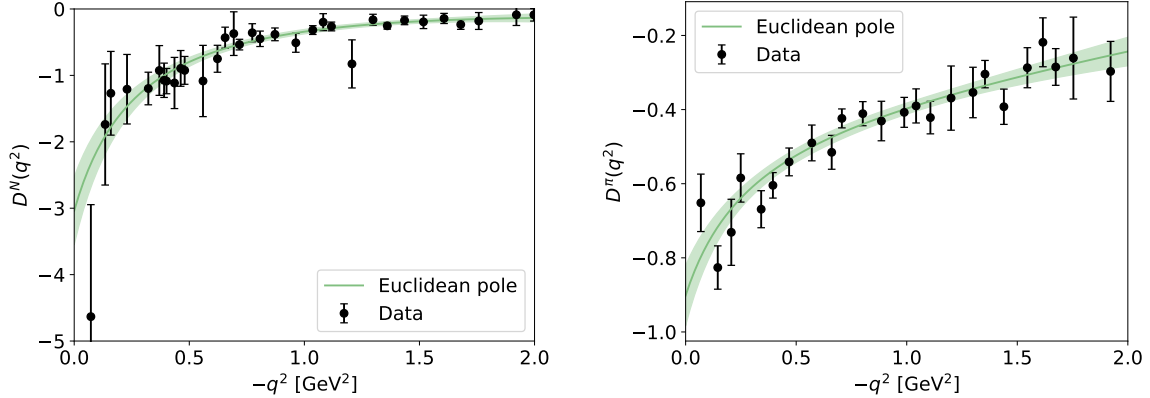


Figure 1: The D -form factors are fitted using a Euclidean pole parametrisation (4.1) and (4.6) with $m_{E,\sigma} = 550$ MeV. The fits are compared to the lattice data, shown in black, for the nucleon [16] (left) and for the pion [17] (right). The dark curve indicates the central fit, while the shaded band represents the 68% confidence interval.

Following the discussion in section 3.1, and particularly in our explorations within the linear σ -model in appendix A.4, this should not come as a surprise. The complex-valued residue at the pole and the effective residue in the Euclidean region are simply not the same quantity. Hence, the two values in (4.5) might well originate from the same underlying theory.

4.2. The pion gravitational form factor

For the pion gravitational form factor we adopt the ansatz

$$D^\pi(q^2) = \frac{q^2 r_{E,\sigma}^\pi}{q^2 - m_{E,\sigma}^2} - 1 + \hat{b} + b' q^2 + \frac{r_{\text{eff}}}{q^2 - m_{\text{eff}}^2}, \quad (4.6)$$

where both the prefactor q^2 in the numerator and the -1 term are dictated by the soft-pion theorem (2.12). This provides a robust constraint, subject only to chiral corrections, implying that

$$\text{soft-pion theorem} \quad \Rightarrow \quad \hat{b} - \frac{r_{\text{eff}}}{m_{\text{eff}}^2} = 0 \pm 0.1, \quad (4.7)$$

which the fits satisfy. An alternative would be to impose the constraint along with next-to-leading order (NLO) computation in chiral perturbation theory [75].

As in the nucleon case, we set $r_{\text{eff}} = 0$ in the main fit. The theoretical prediction for the residue is $r_\sigma^\pi = 2/3$ (2.8), with uncertainties arising from NLO chiral corrections of order $\mathcal{O}([m_\pi^2 \ln m_\pi]/(4\pi F_\pi)^2)$. In the chiral limit $m_{u,d,s} \rightarrow 0$, the value of F_π decreases by about 10% [91]. Adopting this as a guideline for estimating the residue in the chiral limit, and rounding the uncertainty generously, we arrive at the prediction

$$r_\sigma^\pi|_{\text{dilaton}} = \frac{2}{3} \pm 0.1. \quad (4.8)$$

We apply the same fitting procedure as for the nucleon using all 24 data points of ref. [17], with $N_{\text{dof}} = 21$ since there are three fit parameters. The main fits are shown in Fig. 1 and

$m_{E,\sigma}$ [MeV]	$r_{E,\sigma}^\pi$	\hat{b}	b'	χ^2/N_{dof}
450	0.48(16)	0.070(94)	-0.130(45)	1.23
500	0.50(16)	0.085(87)	-0.116(48)	1.20
550	0.53(16)	0.098(81)	-0.101(51)	1.18
600	0.56(17)	0.109(77)	-0.086(55)	1.16
650	0.59(18)	0.119(73)	-0.070(58)	1.14

Table 2: Same as table 1, but now for the pion data [17] fitted using the parametrisation (4.6). LO dilaton effective theory predicts $r_\sigma^\pi = 2/3$. The correlations between parameters for $m_{E,\sigma} = 550$ MeV are $(\rho_{r\hat{b}}, \rho_{rb'}, \rho_{\hat{b}b'}) = (-0.94, 0.86, -0.65)$.

reported in table 2 for a range of effective σ -masses, with uncertainties represented as in table 1. The dependence on the effective mass is much smaller in this case, and our main fit result is

$$r_{E,\sigma}^\pi = 0.53(16)(3) . \quad (4.9)$$

As for the nucleon, we test robustness by considering different background parametrisations. Fitting with no background is better motivated here, since the constant term is fixed by the soft-pion theorem. Indeed, setting $\hat{b} = b' = r_{\text{eff}} = 0$ yields $r_{E,\sigma}^\pi = 0.8(2)$ with $\hat{\chi}^2 = 1.24$, not far from the fit-result in the table. The same background combinations as in the nucleon case give

- a) $(r_{E,\sigma}, \hat{b})^\pi$: with $r_{E,\sigma}^\pi = 0.80(8)$, $\hat{b} = -0.006(62)$ and $\hat{\chi}^2 = 1.30$
- b) $(r_{E,\sigma}, \hat{b}, r_{\text{eff}})^\pi$: with $r_{E,\sigma}^\pi = 0.08(33)$, $\hat{b} = 0.93(42)$, $r_{\text{eff}} = 0.77(34)$ and $\hat{\chi}^2 = 1.12$
- c) $(r_{E,\sigma}, r_{\text{eff}})^\pi$: with $r_{E,\sigma}^\pi = 0.81(4)$, $r_{\text{eff}} = 0.02(5)$ and $\hat{\chi}^2 = 1.29$
- d) $(r_{E,\sigma}, b', r_{\text{eff}})^\pi$: with $r_{E,\sigma}^\pi = 0.58(13)$, $b' = -0.11(6)$, $r_{\text{eff}} = -0.09(8)$ with $\hat{\chi}^2 = 1.19$

First, it is reassuring, and a good indication of the quality of the data, that all fits satisfy the model-independent soft-pion theorem constraint (4.7). Second, with the exception of case b), all fits are compatible with our main result, especially once the spread in $m_{E,\sigma}$ is taken into account. Case c) adds little compared to the no-background fit, since its single parameter is effectively constrained to be small by the soft-pion condition.

The situation is different for case b). Unlike for the nucleon, the extracted residue is not compatible with the dilaton prediction. This indicates that the converse approach, establishing σ -dominance directly, is not feasible for the pion. Rewriting the result as per footnote 4, one finds a residue of $m_\sigma^2 \approx 0.3 \text{ GeV}^2$, far smaller than both the nucleon residue (4.2) and the potential $f_0(980)$ contribution in the pion case. This outcome is therefore not surprising and also explains why the fits are less sensitive to the effective mass $m_{E,\sigma}$ than in the nucleon case.

In conclusion, we find that the pion fits are overall consistent with the dilaton interpretation within uncertainties, although, unlike in the nucleon case, the σ -dominance hypothesis cannot be inferred.

4.3. A quick note on the D -form factor in the infrared - the D -term

As previously discussed, conserved-current form factors are often connected with simple physical interpretations in the infrared. For instance, the gravitational form factors satisfy $A(0) = 1$ and $J(0) = \frac{1}{2}$, reflecting their association with energy and angular momentum. By contrast, an interpretation of the D -form factor has long been elusive; for reviews, see [3, 6]. Particular emphasis has been given to $D \equiv D(0)$, commonly referred to as the D -term (or Druck-term). Viewing the σ -meson as a dilaton, combined with phenomenological fits, provides a new perspective on this longstanding problem.

If the σ were to become massless in the chiral limit, the nucleon D -form factor develops a pole (2.8),

$$D^N(q^2) = \frac{4}{3} \frac{m_N^2}{q^2} + \mathcal{O}(1), \quad (4.10)$$

as emphasised earlier. While this scenario is generally not considered likely, there is also no definitive evidence ruling it out, and recent $N_f = 4$ quark-mass-degenerate lattice simulations do certainly not exclude a massless σ [55].⁶

In the real world, where the σ acquires a nonzero mass, at least due to light quarks, the pole disappears and the D -term remains finite. In the Breit frame, the D -term can be expressed in terms of the pressure and shear forces [40]. When supplemented with the assumption of mechanical stability [96], this formulation implies $D < 0$ (or even $D < -0.20(2)$ [97]), a feature observed in many hadronic systems though not, for example, in hydrogen [98–100]; see [6] for a thorough review. In our approach we obtain (3.8),

$$D \equiv D^N(0) = -\frac{r_{\text{E},\sigma}^N}{m_{\text{E},\sigma}^2} + b(0), \quad (4.11)$$

and with

$$r_{\text{E},\sigma}^N \approx r_\sigma^N = \frac{4}{3} \bar{m}_N^2 > 0, \quad (4.12)$$

one infers that the σ -contribution to the nucleon D -term is necessarily negative. Our fit yields $D^N(0)|_{\text{fit}} = -3.0(5)(3)$ (with the second uncertainty corresponding to the $m_{\text{E},\sigma}$ -variation) which breaks up into a σ - and a background-contribution as $D^N(0)|_{\sigma,\text{fit}} = -3.74(86)(66)$ and $b(0)|_{\text{fit}} = 0.68(35)$ (cf. table 1), and our dilaton prediction for the σ -contribution is $D^N(0)|_\sigma = -3.01(39)$ (4.2). This leads to the conclusion that, provided the σ -meson dominates over the background, the nucleon D -term is negative.

Other values obtained from the lattice data include the z -expansion fit $D = -3.35(58)$ in the original paper [16] and $D = -3.0(4)$ from a constrained tripole-fit [29]. Furthermore, a dispersive analysis at physical pions mass was used to obtain a value of $D = -3.38_{-0.35}^{+0.34}$ [28]. The close agreement among these results is reassuring. However, our main point is not the value but that the σ -contribution is necessarily negative in the dilaton picture, and if dominant over the background, it implies a negative D -term. It is in this respect that our work differs from others.

The D -term is also sought after since it enters the radii associated with the energy-momentum tensor. The mean square radius in the Breit-frame and the mass radius read [3]

$$\langle r_\Theta^2 \rangle = 6A'(0) - \frac{9}{2m_N^2} D, \quad \langle r_{\text{mass}}^2 \rangle = 6A'(0) - \frac{3}{2m_N^2} D, \quad (4.13)$$

⁶See also [94] for functional methods or holographic approaches [95].

respectively. From (4.11) we infer that the σ -contribution (being nonchalent, in distinguishing m_N and \bar{m}_N) is inversely proportional to the effective σ -mass

$$\langle r_{\Theta}^2 \rangle |_{\sigma} = 6(A'(0) + \frac{1}{m_{E,\sigma}^2} - \frac{3}{4} \frac{b(0)}{m_N^2}). \quad (4.14)$$

Thus the mass radii gets larger as the effective σ -mass decreases. This is intuitive and analogous to the pion charge radius, although there the dependence is only logarithmic on the pion mass [67].

What about the D -term for other hadrons? For non-Goldstone states the same pattern applies, see (1.2). In particular, we find similar behaviour for the gluonic gravitational form factors of the ρ -meson and the Δ -baryon [101], based on lattice data at $m_{\pi} \approx 450$ MeV [15]. Let us turn to the Goldstone case. For the pion, the soft-pion theorem requires $D^{\pi}(0) = -1$ [75]. However, in the presence of a massless σ , this relation is modified to $D^{\pi}(0) = -\frac{1}{3}$ [71], as follows directly from (2.8), since the dilaton pole prevents a naive application of the soft-pion theorem.⁷

5. Conclusions and Discussion

In this work, we have fitted the pion and the nucleon gravitational form factors, from lattice QCD data [16, 17], to a parametrisation (3.8) where the σ -meson plays a central role. The main quantity of interest is the residue $r_{E,\sigma}$ of the effective σ -pole which we compare to the dilaton effective theory predictions (2.8). The fit ansatz was motivated theoretically and tested specifically in the linear σ -model which served as a toy model, allowing us to understand the difference between the complex-valued and the effective Euclidean residue.

For the nucleon, we find that the fitted σ -residue is compatible with the dilaton effective theory prediction within uncertainties. Specifically, Eqs. (4.4) and (4.2) are

$$r_{E,\sigma}^N = 1.13(26)(20) \text{ GeV}^2, \quad r_{\sigma}^N |_{\text{dilaton}} = 0.91(12) \text{ GeV}^2, \quad (5.1)$$

the best fit and the dilaton prediction, which are compatible with each other. The first uncertainty arises from the lattice data, and the second estimates the model-uncertainty by varying the effective σ -mass. Additionally, different background parametrisations confirm the robustness of this result, and although extra terms can partially mimic the role of the σ -pole, the extracted residue remains stable within uncertainties.

For the pion, the fits show firm agreement with the model-independent soft-pion theorem (2.12). As in the case of the nucleon the fitted residue also shows good agreement with the dilaton effective theory. This time, Eqs. (4.9) and (4.8) are

$$r_{E,\sigma}^{\pi} = 0.53(16)(3), \quad r_{\sigma}^{\pi} |_{\text{dilaton}} = \frac{2}{3} \pm 0.1, \quad (5.2)$$

the best fit and the dilaton prediction. The uncertainties are of the same type as for the nucleon. Importantly, while the data are consistent with a dilaton-like residue, the converse, establishing σ -dominance directly from the lattice results, is not feasible. This might well be

⁷For a massive σ , one gets $D^{\sigma}(0) = -\frac{3+2\Delta_{\mathcal{O}}}{3}$ with $\Delta_{\mathcal{O}}$ the scaling dimension the mass generating operator \mathcal{O} . If $\mathcal{O} = m_q \bar{q}q$ then $\Delta_{\mathcal{O}} = 2$ and $D^{\sigma}(0) = -\frac{7}{3}$. For a massless σ , one has $D^{\sigma}(0) = -\frac{1}{3}$ as for the pion [71].

due to the data and the somewhat small residue of the pion as a Goldstone boson, and does not undermine the overall consistency of the dilaton interpretation.

Overall, our findings support the idea that QCD is governed by an infrared fixed point with the σ -meson becoming a light or massless dilaton (in the limit of vanishing light quark masses). Presumably, the σ -meson plays a key role in understanding the gravitational D -form factor. In its purest form, with a massless σ , the nucleon form factor develops a pole in the infrared $D^N(q^2) = \frac{4}{3} \frac{m_N^2}{q^2} + \mathcal{O}(1)$. For finite σ -mass, relevant to the real world with nonzero quark mass, our analysis in section 4.3 implies that $D^N(0) < 0$ holds, provided that the σ -term dominates.

As seen from Eqs. (5.1) and (5.2), the dominant uncertainties stem from the data. Further progress can be achieved by improving the precision of the data, extending the kinematic q^2 -range and by going to lower quark masses. Other potential directions, are simulating with degenerate quarks (as in beyond-the-Standard-Model studies) or dispersive approaches [28,30]. In the longer term we might hope for competitive information from experiment, including the future electron-ion collider [102]. Another avenue is testing other systems, varying the spin, for which ρ -meson and the Δ -baryon gluonic gravitational form factors are available at $m_\pi \approx 450$ MeV [15]. This comes with its very own set of challenges, partly related to the proton mass decomposition [103] and will therefore be discussed in a forthcoming paper [101].

Acknowledgements: RS and RZ are supported by the STFC via the consolidated grants ST/T000600/1 and ST/X000494/1. We are grateful to Max Hansen, Keh-Fei Liu, Feng-Kun Guo, Mannque Rho, David Schaich and Hanqing Zheng for discussions. A very special thanks go to the MIT-group members Daniel Hackett, Patrick Oare, Phiala Shanahan and especially Dimitra Pefkou for providing us with their form factor data. Analytic computations were performed with FeynCalc [104] and some Passarino-Veltman functions were numerically checked with LoopTools [105] for real kinematics.

A. The Gell-Mann Lévy linear σ -model – a study case

We use the linear σ -model [106] as a toy model to illustrate the treatment of particles with a sizeable width, thereby providing a basis for interpreting the fit ansatz of Eq. (3.8). Prior to discussing the underlying physics of the linear σ -model and the details of the corresponding calculation, we first introduce the relevant nucleon form factor $F(q^2)$ ⁸

$$\langle N(p') | \sigma | N(p) \rangle = \frac{1}{2m_N^2} \bar{u}(p') F(q^2) u(p), \quad q = p' - p. \quad (\text{A.1})$$

The LO expression is governed by $g = g_{\sigma NN}$, the coupling of the σ to two nucleons,

$$F(s)|_{\text{LO}} = \frac{2m_N^2 g}{s - m_\sigma^2}. \quad (\text{A.2})$$

The NLO form factor can be parameterised as

$$F(s)|_{\text{NLO}} = \frac{2m_N^2 g(1 + v(s))}{s - m_\sigma^2 - \Sigma(s)}, \quad (\text{A.3})$$

where $\Sigma(s)$ and $v(s)$ are the self-energy and the vertex corrections, respectively.

⁸We may regard this form factor as a toy model for the improvement term $T_{\mu\nu} \supset \frac{1}{3}(\partial_\mu \partial_\nu - \eta_{\mu\nu} \partial^2)\sigma$ (2.4).

In the following, we define the model, present the NLO computation, and carry out the analytic continuation. We then use the result to assess the impact of the broad σ -resonance on the form factor parameterisation.

A.1. The linear σ -model Lagrangian in the broken phase

The linear σ -model is a most formidable model, first introduced by Schwinger [107] to implement $SU(2)_L \times SU(2)_R$ invariance in the strong-interaction sector. It was then refined by Gell-Mann and Lévy [106] to include the mechanism of spontaneous symmetry breaking, which leads to massless pions and mass generation of the nucleon, referred to as the Yukawa-mechanism. The renormalisation was worked out in ref. [108], providing an important precursor to the renormalisation of the electroweak sector of the Standard Model. It should be emphasised that the σ -particle, in this context, is not to be confused with the σ -meson of dilaton chiral perturbation theory. In fact, integrating out a potentially heavy σ , in the linear model, leads to chiral perturbation theory, i.e. the *non-linear* σ -model. This allows to determine the low energy constants explicitly. Gasser and Leutwyler [109] make the point that, since the predictions differ from the values observed in nature, the linear σ -model cannot be considered a viable theory of the strong interactions.

The Gell-Mann Lévy linear σ -model with pion mass [106], reads

$$\mathcal{L} = \frac{1}{2}(\partial\pi)^2 + \frac{1}{2}(\partial\sigma)^2 - \frac{1}{2}m_\sigma^2\sigma^2 + \bar{N}(i\not{\partial} - g(\sigma - i\pi\gamma_5))N - V(\sigma, \pi), \quad (\text{A.4})$$

where $\pi = \pi^a T^a$ is understood in the pion to nucleon coupling and the potential is given by $V(\sigma, \pi) = \lambda/4(\sigma^2 + \pi^2 - v^2)^2 - H\sigma$, where $\pi^2 = \pi^a\pi^a$, and H is the (pion) mass perturbation. The potential is minimised by $\partial_\sigma V(F_\pi, 0) = 0$, where F_π differs from v by the perturbation

$$F_\pi^2 = v^2 + \frac{H}{\lambda F_\pi}. \quad (\text{A.5})$$

The vacuum expectation value $\langle\sigma\rangle = F_\pi$ spontaneously breaks the global symmetry $SU(2)_L \times SU(2)_R$ down to the isospin subgroup $SU(2)_V$, with the pions emerging as the associated Goldstone bosons. The constant F_π is identified with the pion decay constant, defined through the axial current matrix element $\langle 0|A_\mu^a|\pi^b\rangle = ip_\mu F_\pi$. The new potential then reads

$$V(\sigma + F_\pi, \pi) = \frac{\lambda}{4}((\sigma + F_\pi)^2 + \pi^2 - v^2)^2 - H(\sigma + F_\pi), \quad (\text{A.6})$$

from where the masses

$$\begin{aligned} m_\pi^2 &= \lambda(F_\pi^2 - v^2) = \frac{H}{F_\pi}, \\ m_\sigma^2 &= \lambda(3F_\pi^2 - v^2) = 2\lambda F_\pi^2 + m_\pi^2, \\ m_N^2 &= g^2 F_\pi^2, \end{aligned} \quad (\text{A.7})$$

and couplings ($V \supset \lambda_n \sigma^n$)

$$\lambda_4 = \frac{\lambda}{4}, \quad \lambda_3 = \lambda F_\pi, \quad g_{\sigma NN} = -g_{\pi NN} = g, \quad (\text{A.8})$$

can be read off. We see that the nucleon mass is generated by a Yukawa mechanism, the pion mass by the explicit breaking term H , and the σ mass is governed by λ and the explicit breaking. The model has four free parameters which we choose to be

$$(g, \lambda, m_\pi, F_\pi) . \quad (\text{A.9})$$

The renormalisation [108] of the linear σ -model is involved, but since we do not aim to match it to experiment we may adapt the $\overline{\text{MS}}$ -scheme within dimensional regularisation. In fact, we slightly modify it for the self-energies to cancel tadpole diagrams (for $\mu = m_\sigma$), so that we may simply ignore them. The concrete values used for (A.9) will be discussed in section A.4.

A.2. Relevant NLO corrections

Our next task is to compute the NLO corrections (A.3). This includes the self-energy and the vertex correction which determine the pole position and the complex residue, respectively. The results are evaluated in terms of Passarino-Veltman functions, defined by

$$I_n(\ell_1^2, \ell_2^2, \dots) = \frac{\mu^{4-d}}{i\pi^{\frac{d}{2}}} \int \frac{d^d k}{(k^2 - m_0^2 + i0)((k + \ell_1)^2 - m_1^2 + i0)((k + \ell_1 + \ell_2)^2 - m_2^2 + i0) \dots} ,$$

where $A_0 = I_0$, $B_0 = I_1$ and $C_0 = I_2$. For the momentum routing of the triangle function C_0 we use the LoopTools conventions [105].

A.2.1. Self-energy corrections $\Sigma(s)$

The goal of this section is to determine the σ -pole, on the second sheet, from the (inverse) propagator

$$\Delta^{-1}(s) = s - m_\sigma^2 - \Sigma(s) . \quad (\text{A.10})$$

We decompose the self-energy into parts

$$\Sigma(s) = \Sigma_{\lambda_3}(s) + \Sigma_{\lambda_4}(s) + \Sigma_g(s) , \quad (\text{A.11})$$

proportional to the couplings λ_3 , λ_4 and g as given in Eq. (A.8), with the $\Sigma_{\lambda_3, g}$ -contributions shown in Fig. 2. An explicit evaluation of all NLO diagrams gives

$$\begin{aligned} \Sigma_{\lambda_3}(s) &= \frac{(\lambda_3)^2}{16\pi^2} (-2(N_f^2 - 1)B_0(s, m_\pi^2, m_\pi^2) - 18B_0(s, m_\sigma^2, m_\sigma^2)) , \\ \Sigma_{\lambda_4}(s) &= \frac{\lambda_4}{16\pi^2} (-12A_0(m_\sigma^2) - 2(N_f^2 - 1)A_0(m_\pi^2)) , \\ \Sigma_g(s) &= \frac{g^2}{16\pi^2} 4N_f ((2m_N^2 - s/2)B_0(s, m_N^2, m_N^2) + A_0(m_N^2)) , \end{aligned} \quad (\text{A.12})$$

where the number of fermions is $N_f = 2$ (proton and neutron).

We start by expressing (A.10) directly in terms of renormalised quantities,

$$\Delta^{-1}(s) = s - m_\sigma^2 - \bar{\Sigma}_{\lambda_3}(s) - \bar{\Sigma}_{\lambda_4}(s) - \bar{\Sigma}_g(s) , \quad (\text{A.13})$$

where the bars indicate that we work in the $\overline{\text{MS}}$ scheme without tadpoles, meaning that A_0, B_0 in (A.12) are replaced by

$$\bar{A}_0(m_a^2) = m_a^2 \left(1 - \ln \frac{m_a^2}{\mu^2} \right) , \quad \bar{B}_0(s, m_a^2, m_a^2) = 2 - \ln \frac{m_a^2}{\mu^2} - \beta_a \ln \left(\frac{\beta_a + 1}{\beta_a - 1} \right) , \quad (\text{A.14})$$

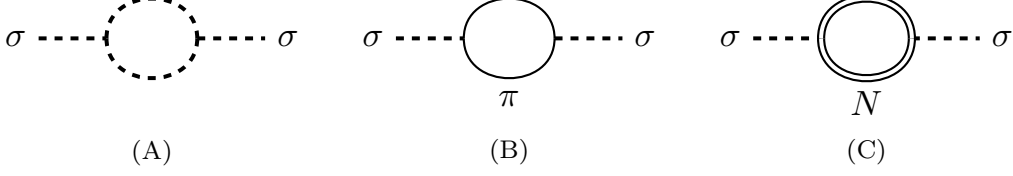


Figure 2: Diagrams for the self-energy corrections $\Sigma_{\lambda_{3,g}}$. The two diagrams for Σ_{λ_4} are not shown.

with $\beta_a = \sqrt{1 - 4m_a^2/s}$, as usual. The σ -pole is then obtained by analytically continuing the inverse propagator to the second sheet,

$$(\Delta^{(II)}(s_\sigma))^{-1} = 0, \quad (\text{A.15})$$

where continuity across the cut is imposed via $(\Delta^{-1})^{(II)}(s - i0) = \Delta^{-1}(s + i0)$. Among the loop functions, only the pion \bar{B}_0 requires a non-trivial continuation

$$\bar{B}_0^{(II)}(s, m_\pi^2, m_\pi^2) = 2 - \ln \frac{m_\pi^2}{\mu^2} - \beta_\pi(s) \ln \frac{1 + \beta_\pi(s)}{1 - \beta_\pi(s)} - i\pi, \quad (\text{A.16})$$

which contributes a large part the imaginary part of s_σ . Equation (A.15) can be solved numerically, or alternatively approximated perturbatively by substituting $s = m_\sigma^2$ into the self-energy⁹

$$s_\sigma = m_\sigma^2 + \bar{\Sigma}_{\lambda_3}^{(II)}(m_\sigma^2) + \bar{\Sigma}_{\lambda_4}^{(II)}(m_\sigma^2) + \bar{\Sigma}_g^{(II)}(m_\sigma^2). \quad (\text{A.17})$$

In practice, we use the numerical solution of (A.13) on the second sheet, which generally yields results close to the analytic approximation.

A.2.2. Vertex corrections $v(s)$

The diagrams for the vertex corrections, in the order shown in Fig. 3, are

$$\begin{aligned} \langle N|\sigma|N \rangle|_{NLO} &= \frac{6ig^2\lambda_3}{s - m_\sigma^2} \int \frac{d^4k}{(2\pi)^4} \bar{u}(p') S_N(k) u(p) \Delta_\sigma(k - p') \Delta_\sigma(k - p) \\ &+ \frac{-6ig^2\lambda_3}{s - m_\sigma^2} \int \frac{d^4k}{(2\pi)^4} \bar{u}(p') \gamma_5 S_N(k) \gamma_5 u(p) \Delta_\pi(k - p') \Delta_\pi(k - p) \\ &+ \frac{ig^3}{s - m_\sigma^2} \int \frac{d^4k}{(2\pi)^4} \bar{u}(p') S_N(k - p) S_N(k - p') u(p) \Delta_\sigma(k). \end{aligned} \quad (\text{A.18})$$

with standard scalar and fermion propagators $\Delta_\sigma(k) = \frac{1}{k^2 - m_\sigma^2}$ and $S_N(k) = \frac{k + m_N}{k^2 - m_N^2}$. The form factor or vertex corrections are obtained by matching to (A.1)

$$F(s) = 2m_N^2 \langle N|\sigma|N \rangle|_{\bar{u}u}, \quad v(s) = \frac{1}{g} (s - m_\sigma^2) \langle N|\sigma|N \rangle|_{\bar{u}u}, \quad (\text{A.19})$$

where $|\bar{u}u$ denotes the projection onto the spinors. We find

$$16\pi^2 v(s) = \frac{6\lambda m_N^2}{s - 4m_N^2} (P_-(m_\sigma^2) C_0(s, m_\sigma^2) + 2\Delta B_0(s, m_\sigma^2, m_\sigma^2))$$

⁹This expression coincides with Eq. (1) in [110], up to the choice of scheme and with the Σ_g term omitted.

$$\begin{aligned}
& + \frac{6\lambda m_N^2}{s - 4m_N^2} (P_+(m_\pi^2)C_0(s, m_\pi^2) + 2\Delta B_0(s, m_\pi^2, m_\pi^2)) \\
& - g^2(B_0(s, m_N^2, m_N^2) + m_\sigma^2 c_0(s, m_\sigma^2)) , \tag{A.20}
\end{aligned}$$

with $P_\pm(\zeta^2) = (4m_N^2 - 2\zeta^2) \pm (s - 4m_N^2)$ making the chirality structure manifest,

$$\Delta B_0(s, m_\sigma^2, m_N^2) = B_0(s, m_\sigma^2, m_\sigma^2) - B_0(m_N^2, m_N^2, m_\sigma^2) , \tag{A.21}$$

which is an ultraviolet-finite contribution, and the abbreviated triangle functions are given by

$$C_0(s, \zeta^2) = C_0(s, m_N^2, m_N^2, \zeta^2, \zeta^2, m_N^2) , \quad c_0(s, \zeta^2) = C_0(s, m_N^2, m_N^2, m_N^2, m_N^2, \zeta^2) .$$

Note that one of the g -factors gets absorbed into $m_N = gv$ in the first two contributions and the singularity at $s = 4m_N^2$ is only apparent; an artefact of the Passarino-Veltman reduction. This means that

$$(4m_N^2 - 2m_\sigma^2)C_0(s, m_\sigma^2) + 2(B_0(s, m_\sigma^2, m_\sigma^2) - B_0(m_N^2, m_N^2, m_\sigma^2)) \Big|_{s=4m_N^2} = 0 , \tag{A.22}$$

must hold which we checked analytically for the imaginary part (using the expressions in the next section) and numerically for the real part.

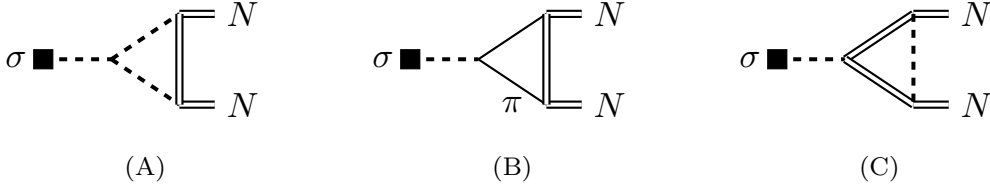


Figure 3: Feynman diagrams for the NLO corrections to the σNN vertex.

A.3. Second-sheet analytic continuation of the form factor

In order to deduce the complex residue we must analytically continue the expression in (A.20) to the second sheet where the pole (A.17) lies. The generic analytic continuation for a function $f(s)$, defined on the first sheet, reads

$$f^{(II)}(s) = f(s) + \text{disc}[f(s)] , \tag{A.23}$$

where $\text{disc}[f(s)] = f(s+i0) - f(s-i0)$ ensures continuity across the cut, $f^{(II)}(s-i0) = f(s+i0)$. Concretely, we have the imaginary parts of the Passarino-Veltman functions analytically, while the real parts can be evaluated numerically through the LoopTools package [105] (for the C_0 function). Fortunately, this proves sufficient since i) the form factors satisfy real analyticity which implies $\text{disc}[f(s)] = 2i\text{Im}f(s)$ by Schwartz's reflection principle and ii) a representation for $f(s)$ valid on the physical sheet is given by the standard dispersion relation

$$f^{(II)}(s) = \frac{1}{\pi} \int ds' \frac{\text{Im}f(s')}{s' - s - i0} + 2i\text{Im}f(s) . \tag{A.24}$$

This expression serves as the master formula for analytic continuation.

The imaginary parts of B_0 and C_0 are provided in Itzykson and Zuber [111], although the expression for C_0 contains significant typos in the Källén function, which we corrected and verified against LoopTools. On the real line we express them as

$$\text{Im}B_0(s, m_1^2, m_2^2) = \pi \frac{\sqrt{\lambda_m}}{s} \theta(s - (m_1 + m_2)^2), \quad (\text{A.25})$$

$$\text{Im}C_0(s, p_1^2, p_2^2, m_1^2, m_2^2, m_3^2) = \frac{-\pi}{\sqrt{\lambda_p}} \ln \frac{a+b}{a-b} \theta(s - (m_1 + m_2)^2), \quad (\text{A.26})$$

where $\lambda_p = \lambda(s, p_1^2, p_2^2)$, $\lambda_m = \lambda(s, m_1^2, m_2^2)$ and $\lambda(s, m_1^2, m_2^2) = (s - (m_1 - m_2)^2)(s - (m_1 + m_2)^2)$ is the Källén function, and

$$a = s^2 - s(p_1^2 + p_2^2 + m_1^2 + m_2^2 - 2m_3^2) - (p_1^2 - p_2^2)(m_1^2 - m_2^2), \quad b = \sqrt{\lambda_p} \sqrt{\lambda_m}. \quad (\text{A.27})$$

For equal masses one has $\text{Im}B_0(s, m_a^2, m_a^2) = \pi \beta_a \theta(s - 4m_a^2)$ which is most often required.

Concretely, for $C_0(s, \zeta^2)$ and similarly for $c_0(s, \zeta^2)$,

$$C_0^{(II)}(s, \zeta^2) = \int_{4\zeta^2}^{\infty} \frac{ds' \frac{1}{\pi} \text{Im}C_0(s', \zeta^2)}{s' - s} + 2i \text{Im}C_0(s, \zeta^2), \quad (\text{A.28})$$

gives a formula valid on the second sheet (away from the cut). For the second type of term we need a once-subtracted dispersion relation

$$\Delta B_0^{(II)}(s, \zeta^2, \zeta^2) = \Delta B_0(s_0, \zeta^2, \zeta^2) + (s - s_0) \int_{4\zeta^2}^{\infty} \frac{ds' \frac{1}{\pi} \text{Im}B_0(s', \zeta^2, \zeta^2)}{(s' - s)(s' - s_0)} + 2i \text{Im}B_0(s, \zeta^2, \zeta^2). \quad (\text{A.29})$$

where $\text{Im}\Delta B_0(s, \zeta^2, \zeta^2) = \text{Im}B_0(s, \zeta^2, \zeta^2)$ has been used. We will choose the subtraction point $s_0 = 0$ below the cut $4\zeta^2$ ($\zeta^2 = m_{\pi, \sigma}^2$). A similar formula is applied for $B_0(s, m_N^2, m_N^2)$ which will be shown explicitly in the final result. It should be stressed that the imaginary parts only need to be added for the pion loops since the sigma loops are above the point where s is continued to the second sheet. The explicit subtraction constants are given by

$$\Delta B_0(0, m^2, m_N^2) = \int_0^1 dx \ln\left(\frac{m_N^2}{m^2} x^2 + (1-x)\right), \quad \bar{B}_0(0, m^2, m^2) = -\ln \frac{m^2}{\mu^2}. \quad (\text{A.30})$$

We note that the μ -dependence in ΔB_0 vanishes between the two terms since the difference is ultraviolet-finite. For \bar{B}_0 , the μ -dependence remains and can be used to assess the uncertainty. The analytic continuation of (A.20), valid on the entire second sheet, reads

$$\begin{aligned} 16\pi^2 v^{(II)}(s) = & \frac{6\lambda m_N^2}{s - 4m_N^2} \left(2(\Delta B_0(0, m_\sigma^2, m_N^2) + s \int_{4m_\sigma^2}^{\infty} \frac{ds' \frac{1}{\pi} \text{Im}B_0(s', m_\sigma^2, m_\sigma^2)}{s'(s' - s)}) \right. \\ & + P_-(m_\sigma^2) \int_{4m_\sigma^2}^{\infty} \frac{ds' \frac{1}{\pi} \text{Im}C_0(s', m_\sigma^2)}{s' - s} + \{m_\sigma \rightarrow m_\pi, P_- \rightarrow P_+\} \\ & \left. + i[4\text{Im}B_0(s, m_\pi^2, m_\pi^2) + 2P_+(m_\pi^2)\text{Im}C_0(s, m_\pi^2)] \right) \\ & - g^2 \left(\bar{B}_0(0, m_N^2, m_N^2) + s \int_{4m_N^2}^{\infty} \frac{ds' \frac{1}{\pi} \text{Im}B_0(s', m_N^2, m_N^2)}{s'(s' - s)} + m_\sigma^2 \int_{4m_N^2}^{\infty} \frac{ds' \frac{1}{\pi} \text{Im}c_0(s', m_\sigma^2)}{s' - s} \right), \end{aligned} \quad (\text{A.31})$$

with the constant functions as per (A.30) and the previously given imaginary parts above. The term in square brackets is due to analytic continuation across the two-pion threshold.

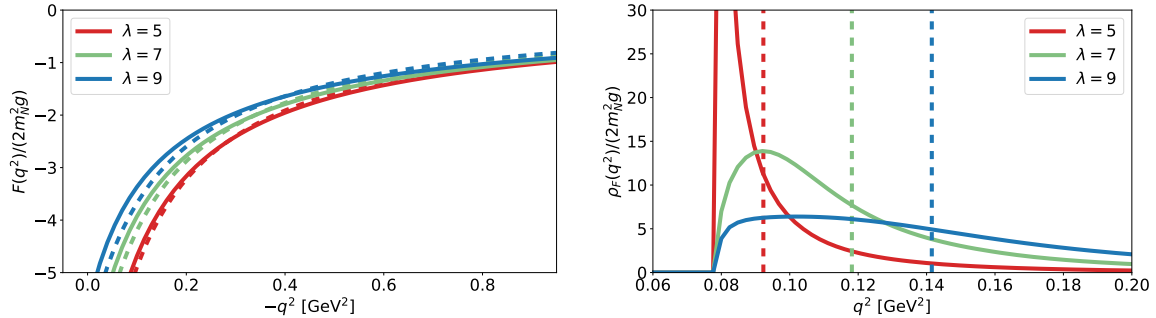


Figure 4: The NLO form factor $F(q^2)$ (A.3) (left) and the corresponding density $\rho_F(s) = \frac{1}{\pi}\text{Im}F(s)$ (right). The input values (A.9) are $m_\pi = 140$ MeV, $F_\pi = 93$ MeV and $\lambda = (g+1/2)^2$ for three different value of λ . The solid lines corresponds to the analytic linear σ -model computation and the dashed lines are fitted effective pole representations (A.33). The linear σ -model and effective pole curves are nearly identical in the Euclidean, despite rather different densities in the Minkowski region.

A.4. Concluding the form-factor study in the linear σ -model

We now return to the investigation of the form factor in the linear σ -model and assess whether the Euclidean ansatz in (3.8) provides a reliable description, and to what extent the complex residue r_σ differs from its Euclidean counterpart $r_{E,\sigma}$. The form factor $F(q^2)$ (A.1) satisfies the standard dispersion relation

$$F(q^2) = \int_{\text{cut}} ds \frac{\rho_F(s)}{s - q^2 - i0}, \quad (\text{A.32})$$

with $\rho_F(s) = \frac{1}{\pi}\text{Im}F(s)$ due to real analyticity. The plot in Fig. 4 demonstrates that the form factor is well approximated by an effective mass $m_{E,\sigma}$, fitted in the range $q^2 \in [-2.95, 0.05]$ GeV²

$$F(q^2)|_{q^2 < 0} = 2m_N^2 g \frac{r_{E,\sigma}}{q^2 - m_{E,\sigma}^2}, \quad (\text{A.33})$$

with $m_{E,\sigma}$ is close to the centre of the ρ_F -distribution, as one would expect. The difference to the generic case (3.6) is that here there is only the pole contribution. In a calculable model, however, such contributions can be separated and are thus not of primary concern. We next compare the complex residue with the effective Euclidean one. The former can be obtained from

$$r_\sigma = \lim_{q^2 \rightarrow s_\sigma} (q^2 - s_\sigma) F^{(II)}(q^2) = 1 + v^{(II)}(s_\sigma), \quad (\text{A.34})$$

where s_σ is the complex pole and $v^{(II)}$ refers to the analytic continuation (A.20).

For illustration we adopt the QCD-inspired values $F_\pi = 93$ MeV and $m_\pi = 140$ MeV, while varying $\lambda = (g + 1/2)^2$. This choice maintains the hierarchy between scalar and fermionic loop contributions. One can choose other values in the (λ, g) -parameter space but as long as there are no strong cancellations the main characteristics remain unchanged. In fact, tuning as $\lambda = (g + 1/2)^2$ is in line with softening the high-energy behaviour akin to the Regge trajectory in QCD.

λ	$m_\sigma^{\text{LO}} [\text{GeV}]$	$m_{E,\sigma} [\text{GeV}]$	$\delta r_{E,\sigma}^{\text{LO}}$	$\sqrt{s}_\sigma [\text{GeV}]$	δr_σ
3	0.27	0.25	-0.036	$0.24e^{0.6^\circ i}$	$-0.13 + 0.03i$
5	0.33	0.30	-0.059	$0.28e^{-4.8^\circ i}$	$-0.07 + 0.02i$
7	0.38	0.34	-0.084	$0.30e^{-9.7^\circ i}$	$-0.14 - 0.10i$
9	0.42	0.38	-0.112	$0.36e^{-16.1^\circ i}$	$-0.08 - 0.25i$
11	0.46	0.40	-0.142	$0.42e^{-19.1^\circ i}$	$-0.00 - 0.34i$
13	0.49	0.42	-0.174	$0.49e^{-20.7^\circ i}$	$0.07 - 0.40i$
15	0.53	0.44	-0.208	$0.55e^{-21.6^\circ i}$	$0.14 - 0.45i$

Table 3: Comparison of the Euclidean and complex pole parameters as a function of $\lambda = (g + 1/2)^2$. The complex pole is given in polar coordinates, facilitating comparison with the tree-level mass and the Euclidean mass $m_{E,\sigma}$. The residues can be reconstructed by adding unity according to (A.35). The Euclidean values are obtained from fits to form-factor data computed in the linear σ -model at 20 evenly spaced points in the interval $q^2 \in [-2.95, 0.05] \text{ GeV}^2$.

The results, summarised in table 3, are expressed in terms of deviations from the normalised LO residue:

$$r_\sigma = 2m_N^2 g (1 + \delta r_\sigma), \quad r_{E,\sigma} = 2m_N^2 g (1 + \delta r_{E,\sigma}). \quad (\text{A.35})$$

From table 3 we observe that the phases of \sqrt{s}_σ and δr_σ are correlated. At the same time, the ratio $|\delta r_{E,\sigma}/\delta r_\sigma|$ differs significantly from unity, confirming the expectation expressed in section 3.1. In general, one further finds that $|\delta r_{E,\sigma}/\delta r_\sigma| < 1$, while the correlation between $|s_\sigma|$ and $m_{E,\sigma}$ holds qualitatively. We therefore conclude that the complex residue at the pole and the effective Euclidean residue exhibit substantial qualitative differences and should not be compared quantitatively.

B. A Multipole Expansion in Momentum Space

In this appendix, we present a more systematic perspective on the representation given in Eq. (3.6), formulated in the spirit of a multipole expansion. We start by decomposing the density into

$$\rho_G(s) = \rho_\varphi(s) + \rho_b(s), \quad (\text{B.1})$$

where $\rho_{\varphi,b}$ denote the φ -resonance and background contributions, respectively. Next, consider expanding the denominator of the dispersion integral (3.4) around $s = m_{E,\sigma}^2$

$$\frac{1}{s - q^2} = \frac{1}{m_{E,\varphi}^2 - q^2} \left(1 + \sum_{n \geq 0} \epsilon^n \right), \quad \epsilon = \frac{m_{E,\varphi}^2 - s}{m_{E,\varphi}^2 - q^2}. \quad (\text{B.2})$$

If $m_{\text{E},\varphi}^2$ is chosen at the centre of the ρ_φ distribution (cf. Fig. 4), then under the integral one has $\epsilon \ll 1$. Carrying out the dispersion integral, one obtains a series

$$G_\varphi(q^2) = \frac{1}{q^2 - m_{\text{E},\varphi}^2} \left(r_{\text{E},\varphi} + \sum_{n \geq 1} \mathcal{E}_n \right), \quad \mathcal{E}_n = \frac{\Omega_n}{(q^2 - m_{\text{E},\varphi}^2)^n}, \quad (\text{B.3})$$

with moments defined as

$$\Omega_n = \int ds \rho_\varphi(s) (m_{\text{E},\varphi}^2 - s)^n, \quad (\text{B.4})$$

which converge if ρ_φ has finite support. For sufficiently Euclidean q^2 , the hierarchy $|\mathcal{E}_{n+1}/\mathcal{E}_n| \ll 1$ is expected to hold, and in practice this may extend to all $q^2 < 0$. Note that $\Omega_0 = -r_{\text{E},\varphi}$ which explains the change in sign in the main q^2 -denominator. This expansion is analogous to the multipole expansion in classical electrodynamics, though here it takes place in momentum rather than coordinate space. The analogue of the charge-distribution centre is played by $m_{\text{E},\varphi}$, the approximate centre of the $\rho_\varphi(s)$ -distribution. The table and figure in appendix A.4 show that the assertions made are true in the linear σ -model for specific parameter ranges. See also the discussion in section 3.1.

References

- [1] I. Y. Kobzarev and L. B. Okun', "Gravitational Interaction of Fermions," *Zh. Eksp. Teor. Fiz.* **43** (1962) 1904–1909.
- [2] H. Pagels, "Energy-Momentum Structure Form Factors of Particles," *Phys. Rev.* **144** (1966) 1250–1260.
- [3] M. V. Polyakov and P. Schweitzer, "Forces inside hadrons: pressure, surface tension, mechanical radius, and all that," *Int. J. Mod. Phys. A* **33** no. 26, (2018) 1830025, [arXiv:1805.06596 \[hep-ph\]](#).
- [4] V. D. Burkert, L. Elouadrhiri, F. X. Girod, C. Lorcé, P. Schweitzer, and P. E. Shanahan, "Colloquium: Gravitational form factors of the proton," *Rev. Mod. Phys.* **95** no. 4, (2023) 041002, [arXiv:2303.08347 \[hep-ph\]](#).
- [5] C. Lorcé, "Electromagnetic and gravitational form factors of the nucleon," *PoS SPIN2023* (2024) 010, [arXiv:2402.00429 \[hep-ph\]](#).
- [6] C. Lorcé and P. Schweitzer, "Pressure inside hadrons: criticism, conjectures, and all that," *Acta Phys. Polon. B* **56** (2025) 3–A17, [arXiv:2501.04622 \[hep-ph\]](#).
- [7] X.-D. Ji, "Gauge-Invariant Decomposition of Nucleon Spin," *Phys. Rev. Lett.* **78** (1997) 610–613, [arXiv:hep-ph/9603249](#).
- [8] V. D. Burkert, L. Elouadrhiri, and F. X. Girod, "The pressure distribution inside the proton," *Nature* **557** no. 7705, (2018) 396–399.
- [9] B. Duran *et al.*, "Determining the gluonic gravitational form factors of the proton," *Nature* **615** no. 7954, (2023) 813–816, [arXiv:2207.05212 \[nucl-ex\]](#).

- [10] **GlueX** Collaboration, S. Adhikari *et al.*, “Measurement of the J/ψ photoproduction cross section over the full near-threshold kinematic region,” *Phys. Rev. C* **108** no. 2, (2023) 025201, [arXiv:2304.03845 \[nucl-ex\]](#).
- [11] M. Diehl, T. Gousset, B. Pire, and O. Teryaev, “Probing partonic structure in $\gamma^* \gamma \rightarrow \pi \pi$ near threshold,” *Phys. Rev. Lett.* **81** (1998) 1782–1785, [arXiv:hep-ph/9805380](#).
- [12] **Belle** Collaboration, M. Masuda *et al.*, “Study of π^0 pair production in single-tag two-photon collisions,” *Phys. Rev. D* **93** no. 3, (2016) 032003, [arXiv:1508.06757 \[hep-ex\]](#).
- [13] S. Kumano, Q.-T. Song, and O. V. Teryaev, “Hadron tomography in meson-pair production and gravitational form factors,” *PoS SPIN2018* (2019) 074, [arXiv:1902.04333 \[hep-ph\]](#).
- [14] P. E. Shanahan and W. Detmold, “Gluon gravitational form factors of the nucleon and the pion from lattice QCD,” *Phys. Rev. D* **99** no. 1, (2019) 014511, [arXiv:1810.04626 \[hep-lat\]](#).
- [15] D. A. Pefkou, D. C. Hackett, and P. E. Shanahan, “Gluon gravitational structure of hadrons of different spin,” *Phys. Rev. D* **105** no. 5, (2022) 054509, [arXiv:2107.10368 \[hep-lat\]](#).
- [16] D. C. Hackett, D. A. Pefkou, and P. E. Shanahan, “Gravitational Form Factors of the Proton from Lattice QCD,” *Phys. Rev. Lett.* **132** no. 25, (2024) 251904, [arXiv:2310.08484 \[hep-lat\]](#).
- [17] D. C. Hackett, P. R. Oare, D. A. Pefkou, and P. E. Shanahan, “Gravitational form factors of the pion from lattice QCD,” *Phys. Rev. D* **108** no. 11, (2023) 114504, [arXiv:2307.11707 \[hep-lat\]](#).
- [18] χ **QCD** Collaboration, B. Wang, F. He, G. Wang, T. Draper, J. Liang, K.-F. Liu, and Y.-B. Yang, “Trace anomaly form factors from lattice QCD,” *Phys. Rev. D* **109** no. 9, (2024) 094504, [arXiv:2401.05496 \[hep-lat\]](#).
- [19] R. Abbott, D. C. Hackett, D. A. Pefkou, F. Romero-López, and P. Shanahan, “Gravitational form factors of glueballs in Yang-Mills theory,” in *41st International Symposium on Lattice Field Theory*. 10, 2024. [arXiv:2410.02706 \[hep-lat\]](#).
- [20] A. V. Belitsky and X. Ji, “Chiral structure of nucleon gravitational form-factors,” *Phys. Lett. B* **538** (2002) 289–297, [arXiv:hep-ph/0203276](#).
- [21] H. Alharazin, B. D. Sun, E. Epelbaum, J. Gegelia, and U. G. Meißner, “Gravitational $p \rightarrow \Delta^+$ transition form factors in chiral perturbation theory,” *JHEP* **03** (2024) 007, [arXiv:2312.05193 \[hep-ph\]](#).
- [22] I. V. Anikin, “Gravitational form factors within light-cone sum rules at leading order,” *Phys. Rev. D* **99** no. 9, (2019) 094026, [arXiv:1902.00094 \[hep-ph\]](#).
- [23] X.-B. Tong, J.-P. Ma, and F. Yuan, “Gluon gravitational form factors at large momentum transfer,” *Phys. Lett. B* **823** (2021) 136751, [arXiv:2101.02395 \[hep-ph\]](#).

- [24] X.-B. Tong, J.-P. Ma, and F. Yuan, “Perturbative calculations of gravitational form factors at large momentum transfer,” *JHEP* **10** (2022) 046, [arXiv:2203.13493 \[hep-ph\]](#).
- [25] U. Özdem and K. Azizi, “Gravitational transition form factors of $N \rightarrow \Delta$ via QCD light-cone sum rules,” *JHEP* **03** (2023) 048, [arXiv:2212.07290 \[hep-ph\]](#).
- [26] Z. Dehghan, F. Almaksusi, and K. Azizi, “Mechanical properties of proton using flavor-decomposed gravitational form factors,” *JHEP* **06** (2025) 025, [arXiv:2502.16689 \[hep-ph\]](#).
- [27] W. Broniowski and E. Ruiz Arriola, “Gravitational form factors of the pion and meson dominance,” *Phys. Lett. B* **859** (2024) 139138, [arXiv:2405.07815 \[hep-ph\]](#).
- [28] X.-H. Cao, F.-K. Guo, Q.-Z. Li, and D.-L. Yao, “Dispersive determination of nucleon gravitational form factors,” *Nature Commun.* **16** no. 1, (2025) 6979, [arXiv:2411.13398 \[hep-ph\]](#).
- [29] W. Broniowski and E. Ruiz Arriola, “Gravitational form factors and mechanical properties of the nucleon in a meson dominance approach,” [arXiv:2503.09297 \[hep-ph\]](#).
- [30] X.-H. Cao, F.-K. Guo, Q.-Z. Li, B.-W. Wu, and D.-L. Yao, “Gravitational form factors of pions, kaons and nucleons from dispersion relations,” [arXiv:2507.05375 \[hep-ph\]](#).
- [31] C. Cebulla, K. Goeke, J. Ossmann, and P. Schweitzer, “The Nucleon form-factors of the energy momentum tensor in the Skyrme model,” *Nucl. Phys. A* **794** (2007) 87–114, [arXiv:hep-ph/0703025](#).
- [32] J.-H. Jung, U. Yakhshiev, and H.-C. Kim, “Energy–momentum tensor form factors of the nucleon within a π - ρ - ω soliton model,” *J. Phys. G* **41** (2014) 055107, [arXiv:1310.8064 \[hep-ph\]](#).
- [33] M. Tanaka, D. Fujii, and M. Kawaguchi, “Gravitational form factors of the nucleon in the Skyrme model based on scale-invariant chiral perturbation theory,” [arXiv:2507.21220 \[hep-ph\]](#).
- [34] D. Chakrabarti, C. Mondal, A. Mukherjee, S. Nair, and X. Zhao, “Gravitational form factors and mechanical properties of proton in a light-front quark-diquark model,” *Phys. Rev. D* **102** (2020) 113011, [arXiv:2010.04215 \[hep-ph\]](#).
- [35] Y. Choi, H.-D. Son, and H.-M. Choi, “Gravitational form factors of the pion in the self-consistent light-front quark model,” *Phys. Rev. D* **112** no. 1, (2025) 014043, [arXiv:2504.14997 \[hep-ph\]](#).
- [36] K. A. Mamo and I. Zahed, “Nucleon mass radii and distribution: Holographic QCD, Lattice QCD and GlueX data,” *Phys. Rev. D* **103** no. 9, (2021) 094010, [arXiv:2103.03186 \[hep-ph\]](#).
- [37] K. A. Mamo and I. Zahed, “ J/ψ near threshold in holographic QCD: A and D gravitational form factors,” *Phys. Rev. D* **106** no. 8, (2022) 086004, [arXiv:2204.08857 \[hep-ph\]](#).

- [38] S. Sugimoto and T. Tsukamoto, “Energy-Momentum Tensor and D-term of Baryons in Top-down Holographic QCD,” [arXiv:2503.19492 \[hep-th\]](#).
- [39] M. Tanaka, D. Fujii, and A. Iwanaka, “Pion Gravitational Form Factors in Holographic QCD,” [arXiv:2504.01115 \[hep-ph\]](#).
- [40] M. V. Polyakov, “Generalized parton distributions and strong forces inside nucleons and nuclei,” *Phys. Lett. B* **555** (2003) 57–62, [arXiv:hep-ph/0210165](#).
- [41] C. J. Isham, A. Salam, and J. A. Strathdee, “Spontaneous breakdown of conformal symmetry,” *Phys. Lett. B* **31** (1970) 300–302.
- [42] B. Zumino, *Effective Lagrangians and Broken Symmetries*, vol. 2 of *1970 Brandeis University Summer Institute in Theoretical Physics, Vol. 2*. (M.I.T. Press, Cambridge, MA, 1970), Providence, RI, 1970.
- [43] J. R. Ellis, “Phenomenological actions for spontaneously-broken conformal symmetry,” *Nucl. Phys. B* **26** (1971) 536–546.
- [44] R. J. Crewther and L. C. Tunstall, “ $\Delta I = 1/2$ rule for kaon decays derived from QCD infrared fixed point,” *Phys. Rev. D* **91** no. 3, (2015) 034016, [arXiv:1312.3319 \[hep-ph\]](#).
- [45] R. J. Crewther and L. C. Tunstall, “Status of Chiral-Scale Perturbation Theory,” *PoS CD15* (2015) 132, [arXiv:1510.01322 \[hep-ph\]](#).
- [46] R. Zwicky, “QCD with an infrared fixed point: The pion sector,” *Phys. Rev. D* **109** no. 3, (2024) 034009, [arXiv:2306.06752 \[hep-ph\]](#).
- [47] R. Zwicky, “QCD with an infrared fixed point and a dilaton,” *Phys. Rev. D* **110** no. 1, (2024) 014048, [arXiv:2312.13761 \[hep-ph\]](#).
- [48] R. Zwicky, “Soft Theorems and Dilaton Effective Theory,” *PoS LATTICE2024* (2025) 151, [arXiv:2508.16501 \[hep-lat\]](#).
- [49] L. Del Debbio, B. Lucini, A. Patella, C. Pica, and A. Rago, “Large volumes and spectroscopy of walking theories,” *Phys. Rev. D* **93** no. 5, (2016) 054505, [arXiv:1512.08242 \[hep-lat\]](#).
- [50] A. Hasenfratz, C. Rebbi, and O. Witzel, “Gradient flow step-scaling function for SU(3) with ten fundamental flavors,” *Phys. Rev. D* **101** no. 11, (2020) 114508, [arXiv:2004.00754 \[hep-lat\]](#).
- [51] Z. Fodor, K. Holland, J. Kuti, D. Nogradi, and C. H. Wong, “Extended investigation of the twelve-flavor β -function,” *Phys. Lett. B* **779** (2018) 230–236, [arXiv:1710.09262 \[hep-lat\]](#).
- [52] **Lattice Strong Dynamics** Collaboration, T. Appelquist *et al.*, “Nonperturbative investigations of SU(3) gauge theory with eight dynamical flavors,” *Phys. Rev. D* **99** no. 1, (2019) 014509, [arXiv:1807.08411 \[hep-lat\]](#).

- [53] **Lattice Strong Dynamics** Collaboration, R. C. Brower *et al.*, “Light Scalar Meson and Decay Constant in SU(3) Gauge Theory with Eight Dynamical Flavors,” [arXiv:2306.06095 \[hep-lat\]](#).
- [54] E. Bennett, D. K. Hong, H. Hsiao, J.-W. Lee, C. J. D. Lin, B. Lucini, M. Piai, and D. Vadamchino, “Meson spectroscopy in the Sp(4) gauge theory with three antisymmetric fermions,” *Phys. Rev. D* **111** no. 7, (2025) 074511, [arXiv:2412.01170 \[hep-lat\]](#).
- [55] **LatKMI** Collaboration, Y. Aoki, T. Aoyama, E. Bennett, T. Maskawa, K. Miura, H. Ohki, E. Rinaldi, A. Shibata, K. Yamawaki, and T. Yamazaki, “A novel view of the flavor-singlet spectrum from multi-flavor QCD on the lattice,” [arXiv:2505.08658 \[hep-lat\]](#).
- [56] T. Appelquist, J. Ingoldby, and M. Piai, “Dilaton EFT Framework For Lattice Data,” *JHEP* **07** (2017) 035, [arXiv:1702.04410 \[hep-ph\]](#).
- [57] T. Appelquist, J. Ingoldby, and M. Piai, “Analysis of a Dilaton EFT for Lattice Data,” *JHEP* **03** (2018) 039, [arXiv:1711.00067 \[hep-ph\]](#).
- [58] C. Cresswell-Hogg, D. F. Litim, and R. Zwicky, “Dilaton Physics from Asymptotic Freedom,” [arXiv:2502.00107 \[hep-th\]](#).
- [59] J. Terning, *Modern supersymmetry: Dynamics and duality*. 2006.
- [60] M. Shifman and R. Zwicky, “Relating β^* and γ_{Q^*} in the N=1 SQCD conformal window,” *Phys. Rev. D* **108** no. 11, (2023) 114013, [arXiv:2310.16449 \[hep-th\]](#).
- [61] S. Matsuzaki and K. Yamawaki, “Holographic techni-dilaton at 125 GeV,” *Phys. Rev. D* **86** (2012) 115004, [arXiv:1209.2017 \[hep-ph\]](#).
- [62] D. D. Dietrich, F. Sannino, and K. Tuominen, “Light composite Higgs from higher representations versus electroweak precision measurements: Predictions for CERN LHC,” *Phys. Rev. D* **72** (2005) 055001, [arXiv:hep-ph/0505059](#).
- [63] O. Catà, R. J. Crewther, and L. C. Tunstall, “Crawling technicolor,” *Phys. Rev. D* **100** no. 9, (2019) 095007, [arXiv:1803.08513 \[hep-ph\]](#).
- [64] G. E. Brown and M. Rho, “Scaling effective Lagrangians in a dense medium,” *Phys. Rev. Lett.* **66** (1991) 2720–2723.
- [65] M. Rho and Y.-L. Ma, “Manifestation of Hidden Symmetries in Baryonic Matter: From Finite Nuclei to Neutron Stars,” *Mod. Phys. Lett. A* **36** no. 13, (2021) 2130012, [arXiv:2101.07121 \[nucl-th\]](#).
- [66] M. Rho and L.-Q. Shao, “Probing for an IR-fixed Point in QCD by Superaligned Gamow-Teller Transitions in Doubly Magic Nuclei,” [arXiv:2410.04991 \[nucl-th\]](#).
- [67] J. F. Donoghue, E. Golowich, and B. R. Holstein, *Dynamics of the standard model*, vol. 2. CUP, 2014.

- [68] A. Tarasov and R. Venugopalan, “Role of the chiral anomaly in polarized deeply inelastic scattering. III. Wess-Zumino-Witten contributions and chiral Ward identities for finite quark mass,” *Phys. Rev. D* **111** no. 7, (2025) 074027, [arXiv:2501.10519 \[hep-ph\]](#).
- [69] M. Gell-Mann, *Symmetry violation in hadron physics*. 1969.
- [70] L. Del Debbio and R. Zwicky, “Dilaton and massive hadrons in a conformal phase,” *JHEP* **08** (2022) 007, [arXiv:2112.11363 \[hep-ph\]](#).
- [71] R. Zwicky, “Dilatons Improve (Non)-Goldstones,” [arXiv:2306.12914 \[hep-th\]](#).
- [72] G. Mack and A. Salam, “Finite component field representations of the conformal group,” *Annals Phys.* **53** (1969) 174–202.
- [73] C. J. Isham, A. Salam, and J. A. Strathdee, “Broken chiral and conformal symmetry in an effective-lagrangian formalism,” *Phys. Rev. D* **2** (1970) 685–690.
- [74] S. Scherer and M. R. Schindler, *A Primer for Chiral Perturbation Theory*, vol. 830. 2012.
- [75] J. F. Donoghue and H. Leutwyler, “Energy and momentum in chiral theories,” *Z. Phys. C* **52** (1991) 343–351.
- [76] J. R. Pelaez, “From controversy to precision on the sigma meson: a review on the status of the non-ordinary $f_0(500)$ resonance,” *Phys. Rept.* **658** (2016) 1, [arXiv:1510.00653 \[hep-ph\]](#).
- [77] I. Caprini, G. Colangelo, and H. Leutwyler, “Mass and width of the lowest resonance in QCD,” *Phys. Rev. Lett.* **96** (2006) 132001, [arXiv:hep-ph/0512364](#).
- [78] J. F. Donoghue, “Sigma exchange in the nuclear force and effective field theory,” *Phys. Lett. B* **643** (2006) 165–170, [arXiv:nucl-th/0602074](#).
- [79] A. Calle Cordon and E. Ruiz Arriola, “Scalar meson mass from renormalized One Boson Exchange Potential,” *AIP Conf. Proc.* **1030** no. 1, (2008) 334–338, [arXiv:0804.2350 \[nucl-th\]](#).
- [80] B. Wu, X.-H. Cao, X.-K. Dong, and F.-K. Guo, “ σ exchange in the one-boson exchange model involving the ground state octet baryons,” *Phys. Rev. D* **109** no. 3, (2024) 034026, [arXiv:2312.01013 \[hep-ph\]](#).
- [81] S. Weinberg, *The quantum theory of fields. Vol. 2: Modern applications*. Cambridge University Press, 8, 2013.
- [82] H.-q. Zheng, “How to parameterize a light and broad resonance (the sigma meson),” in *International Symposium on Hadron Spectroscopy, Chiral Symmetry and Relativistic Description of Bound Systems*, pp. 98–105. 4, 2003. [arXiv:hep-ph/0304173](#).
- [83] R. Omnes, “On the Solution of certain singular integral equations of quantum field theory,” *Nuovo Cim.* **8** (1958) 316–326.

- [84] B. Moussallam, “Couplings of light $I=0$ scalar mesons to simple operators in the complex plane,” *Eur. Phys. J. C* **71** (2011) 1814, [arXiv:1110.6074 \[hep-ph\]](#).
- [85] M. Hoferichter, C. Ditsche, B. Kubis, and U. G. Meissner, “Dispersive analysis of the scalar form factor of the nucleon,” *JHEP* **06** (2012) 063, [arXiv:1204.6251 \[hep-ph\]](#).
- [86] F. Giacosa, A. Okopińska, and V. Shastry, “A simple alternative to the relativistic Breit–Wigner distribution,” *Eur. Phys. J. A* **57** no. 12, (2021) 336, [arXiv:2106.03749 \[hep-ph\]](#).
- [87] **Hadron Spectrum** Collaboration, A. Rodas, J. J. Dudek, and R. G. Edwards, “Determination of crossing-symmetric $\pi\pi$ scattering amplitudes and the quark mass evolution of the σ constrained by lattice QCD,” *Phys. Rev. D* **109** no. 3, (2024) 034513, [arXiv:2304.03762 \[hep-lat\]](#).
- [88] W.-Y. Liu, E. Shuryak, and I. Zahed, “Pion gravitational form factors in the QCD instanton vacuum. II,” *Phys. Rev. D* **110** no. 5, (2024) 054022, [arXiv:2405.16269 \[hep-ph\]](#).
- [89] S. S. Agaev, V. M. Braun, N. Offen, F. A. Porkert, and A. Schäfer, “Transition form factors $\gamma^*\gamma \rightarrow \eta$ and $\gamma^*\gamma \rightarrow \eta'$ in QCD,” *Phys. Rev. D* **90** no. 7, (2014) 074019, [arXiv:1409.4311 \[hep-ph\]](#).
- [90] M. Hoferichter and J. R. de Elvira, *Nucleon mass: trace anomaly and σ -terms*. 6, 2025. [arXiv:2506.23902 \[hep-ph\]](#).
- [91] **Flavour Lattice Averaging Group (FLAG)** Collaboration, Y. Aoki *et al.*, “FLAG Review 2024,” [arXiv:2411.04268 \[hep-lat\]](#).
- [92] J. Gasser, M. E. Sainio, and A. Svarc, “Nucleons with Chiral Loops,” *Nucl. Phys. B* **307** (1988) 779–853.
- [93] M. Hoferichter, J. R. de Elvira, B. Kubis, and U.-G. Meißner, “Nucleon resonance parameters from Roy–Steiner equations,” *Phys. Lett. B* **853** (2024) 138698, [arXiv:2312.15015 \[hep-ph\]](#).
- [94] F. Goertz, Á. Pastor-Gutiérrez, and J. M. Pawłowski, “Gauge-Fermion Cartography: from confinement and chiral symmetry breaking to conformality,” [arXiv:2412.12254 \[hep-th\]](#).
- [95] D. Elander, A. F. Faedo, M. Piai, R. Rodgers, and J. G. Subils, “Light dilaton near critical points in top-down holography,” [arXiv:2502.19226 \[hep-th\]](#).
- [96] I. A. Perevalova, M. V. Polyakov, and P. Schweitzer, “On LHCb pentaquarks as a baryon- $\psi(2S)$ bound state: prediction of isospin- $\frac{3}{2}$ pentaquarks with hidden charm,” *Phys. Rev. D* **94** no. 5, (2016) 054024, [arXiv:1607.07008 \[hep-ph\]](#).
- [97] J. Gegelia and M. V. Polyakov, “A bound on the nucleon Druck-term from chiral EFT in curved space-time and mechanical stability conditions,” *Phys. Lett. B* **820** (2021) 136572, [arXiv:2104.13954 \[hep-ph\]](#).

- [98] X. Ji, J. Yang, and Y. Liu, “Gravitational tensor-monopole moment of the hydrogen atom to order $O(\alpha)$,” *Phys. Rev. D* **110** no. 11, (2024) 114045, [arXiv:2208.05029 \[hep-ph\]](#).
- [99] A. Czarnecki, Y. Liu, and S. N. Reza, “Energy-momentum Tensor of a Hydrogen Atom: Stability, D -term, and the Lamb Shift,” *Acta Phys. Polon. Supp.* **16** no. 7, (2023) 7–A19, [arXiv:2309.10994 \[hep-ph\]](#).
- [100] A. Freese, “Quantum stresses in the hydrogen atom,” *Phys. Rev. D* **111** no. 3, (2025) 034047, [arXiv:2412.09664 \[hep-ph\]](#).
- [101] R. Stegeman and R. Zwicky, *to appear*.
- [102] A. Accardi *et al.*, “Electron Ion Collider: The Next QCD Frontier: Understanding the glue that binds us all,” *Eur. Phys. J. A* **52** no. 9, (2016) 268, [arXiv:1212.1701 \[nucl-ex\]](#).
- [103] X.-D. Ji, “A QCD analysis of the mass structure of the nucleon,” *Phys. Rev. Lett.* **74** (1995) 1071–1074, [arXiv:hep-ph/9410274](#).
- [104] V. Shtabovenko, R. Mertig, and F. Orellana, “FeynCalc 10: Do multiloop integrals dream of computer codes?,” *Comput. Phys. Commun.* **306** (2025) 109357, [arXiv:2312.14089 \[hep-ph\]](#).
- [105] T. Hahn and M. Perez-Victoria, “Automatized one loop calculations in four and D dimensions,” *Comput. Phys. Commun.* **118** (1999) 153–165, [arXiv:hep-ph/9807565](#).
- [106] M. Gell-Mann and M. Levy, “The axial vector current in beta decay,” *Nuovo Cim.* **16** (1960) 705.
- [107] J. S. Schwinger, “A Theory of the Fundamental Interactions,” *Annals Phys.* **2** (1957) 407–434.
- [108] J.-L. Gervais and B. W. Lee, “Renormalization of the sigma-model (ii) fermion fields and regularization,” *Nucl. Phys. B* **12** (1969) 627–646.
- [109] J. Gasser and H. Leutwyler, “Chiral Perturbation Theory to One Loop,” *Annals Phys.* **158** (1984) 142.
- [110] P. Masjuan, J. J. Sanz-Cillero, and J. Virto, “Some Remarks on the Pade Unitarization of Low-Energy Amplitudes,” *Phys. Lett. B* **668** (2008) 14–19, [arXiv:0805.3291 \[hep-ph\]](#).
- [111] C. Itzykson and J. B. Zuber, *Quantum Field Theory*. International Series In Pure and Applied Physics. McGraw-Hill, New York, 1980.